Electronic Supplementary Information (ESI)

Unraveling the Superior Aqueous Na-ion Storage in Multicyano-substituted Phenazine-based Electrode Material

Jing He,[a] Renyuan Wang,[a] Lingyun Li,[a] Liping Zhao,[b] Minjie Shi,[a] and Chao Yan[a*]

[a] School of Materials Science and Engineering, Jiangsu University of Science and Technology, Zhenjiang, 212003, P. R. China

[b] State Key Laboratory for Metallic Matrix Composite Materials, School of Materials Science and Engineering, Shanghai Jiao Tong University, Shanghai 200240, P. R. China

Experimental

Preparation of CDPZ@G

CDPZ organic compound was synthesized by a condensation reaction between hexaketocyclohexane octahydrate and 4,5-diaminophthalonitrile within a mole ratio of 1:3 in an acetic acid solution to reflux for 10 h under an argon atmosphere. Graphene nanosheets were obtained from the ascorbic acid reduction method previously reported.[S1] After that, the CDPZ@G was fabricated by a facile and efficient electrostatic self-assembly method, wherein the CDPZ solution was mixed with the graphene suspension within a CDPZ/graphene mass ratio of 2:1. As a result of remaining still for about 1 h, the supernatant of the mixed solution turned clear, but the precipitate was visible, which was further collected by centrifugation and washing. Finally, the black CDPZ@G powder can be achieved under vacuum drying at 50 °C for 8 h. For comparison, the DPZ@G was synthesized by the same preparation process, in which the DPZ organic compound without cyano substituents was synthesized by the condensation reaction between hexaketocyclohexane octahydrate and o-phenylenediamine.[S2]

Characterization methods

Several techniques were used for evaluating the morphology and microstructure of the synthesized samples, including scanning electron microscope (SEM, FEI, Nova NanoSem450), transmission electron microscope (TEM, TecnaiG220S-Twin), nuclear magnetic resonance spectra (NMR, Bruker Avance III spectrometer, 400 MHz), X-ray photoelectron spectroscopy (XPS, KAlpha Thermo electron), Laser Micro-Raman Spectrometer (Raman; RENISHAW inVia) and Fourier transform infrared (FTIR, Nicolet 6700).

In-situ FTIR investigation

In-situ FTIR measurement of the CDPZ@G electrode was conducted by a custom-made in-situ FTIR electrochemical cell in 10 M NaOH electrolyte with the three-electrode configuration (Fig. S9), in which CDPZ@G electrode was used as the working electrode, and graphite rod and Ag/AgCl electrode were used as the counter and reference electrode, respectively. FTIR spectra were collected in transmittance mode by reflecting the infrared light onto the CDPZ@G electrode with 4 scans at a resolution of 5 cm^{-1} throughout the range from 1000 to 2500 cm^{-1} during the GCD electrochemical testing at a current density of 1.0 C.

Electrochemical measurements

The electrode materials (CDPZ@G or DPZ@G) were prepared by mixing 70 wt% active materials, 20 wt% of acetylene black and 10 wt% polyvinylidenefluoride binders together with the aid of N-methylpyrrolidone solution, and the uniformly mixed slurry was pressed onto the graphite paper and dried under vacuum for 8 h at 80 °C. Using a three-electrode test configuration, the electrochemical properties of electrode materials were evaluated in 10 M NaOH electrolyte. Cyclic voltammetry (CV) and galvanostatic charge/discharge (GCD) measurements were conducted under different scanning rates and current densities, and electrochemical impedance spectroscopy (EIS) was carried out at frequencies from 100 kHz to 0.01 Hz. Specific capacity of CDPZ@G electrode was estimated from the discharge curves by using the following equation:

$$C = \frac{I \cdot \Delta t}{m \cdot 3.6} \qquad (1)$$

where C (mA h g^{-1}) is the specific capacity of the CDPZ@G electrode, I (mA) is the applied discharging current, Δt (s) is the discharging time and m (mg) is the whole mass

of the CDPZ@G electrode.

For the fabrication of a soft-package ANIB device, the resultant CDPZ@G electrode was applied as the anode material, while a two-dimensional conductive Ni-1,2,4,5-benzenetetramine metal-organic framework (2D Ni-MOF) was prepared and used as the cathode material. The CDPZ@G anode, cellulose acetate separator, and 2D Ni-MOF cathode were then carefully packed in a sandwich arrangement (anode-separator-cathode) and encapsulated in aluminum-plastic film for packaging, in which the mass ratio of cathode to anode is 1.5:1. After injecting NaOH aqueous electrolyte, the soft-package ANIB was vacuum sealed with a sealing apparatus.

References

S1 N. Liu, X. Wu, Y. Zhang, Y. Yin, C. Sun, Y. Mao, L. Fan and N. Zhang, *Adv. Sci.*, 2020, **7**, 2000146.

S2 Z. Tie, L. Liu, S. Deng, D. Zhao and Z. Niu, *Angew. Chem. Int. Ed.*, 2020, **59**, 4920.

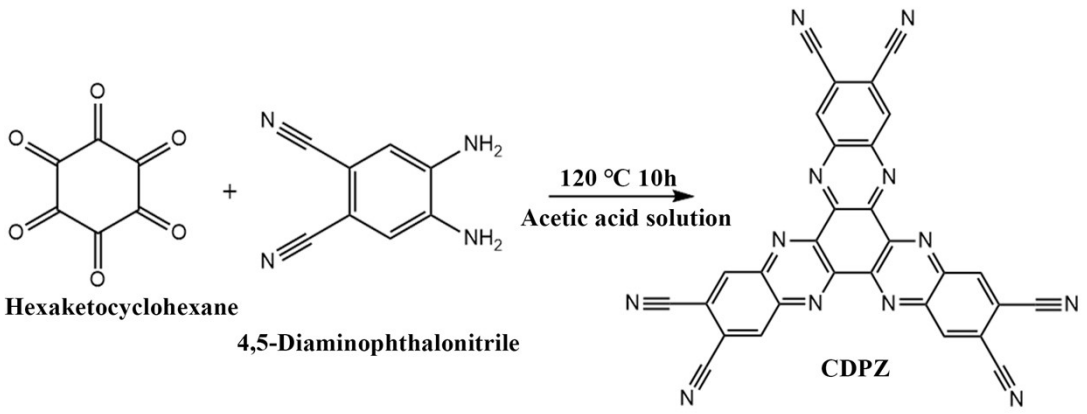

Fig. S1 Schematic illustration of the synthesis reaction for CDPZ organic compound.

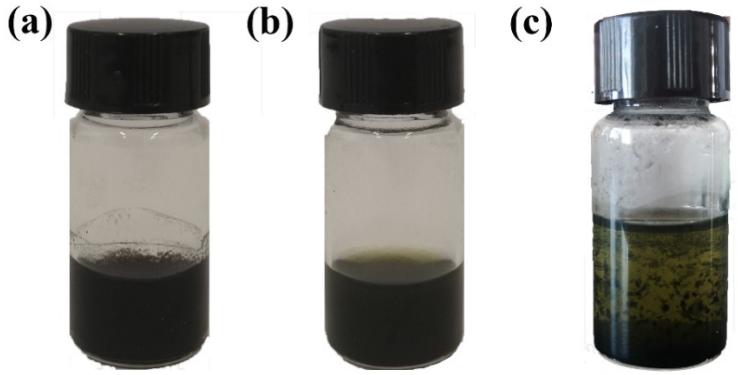

Fig. S2 Digital photos of (a) graphene nanosheets, (b) CDPZ homogeneous suspensions and (c) CDPZ/graphene mixed solution after standing for about 1 h, in which the black precipitate and clear supernatant can be observed owing to the electrostatic self-assembly between CDPZ and graphene nanosheets solutions.

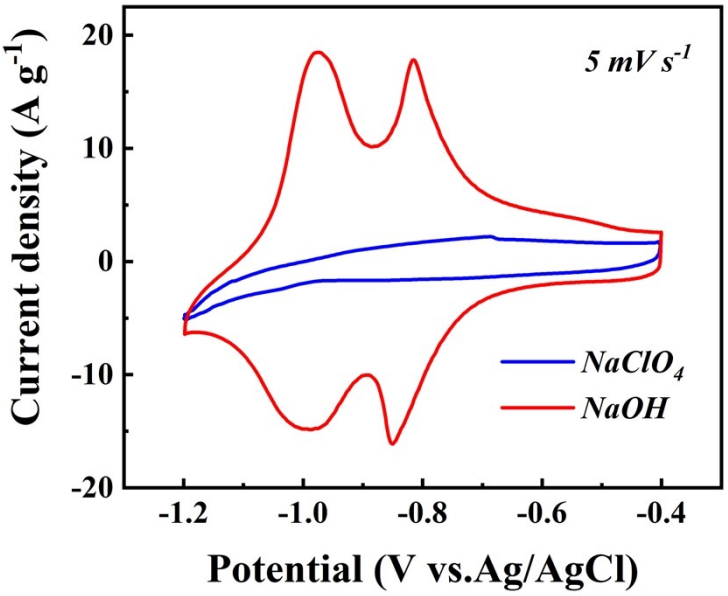

Fig. S3 CV curves of CPDZ@G electrode (Ag/AgCl as reference electrode) in NaOH and $NaClO_4$ aqueous electrolytes.

Fig. S3 displays the CV curve with negligible peaks of CDPZ@G electrode in 10 M $NaClO_4$ aqueous electrolyte, while two pairs of obvious redox peaks can be identified from the CV curve in 10 M NaOH aqueous electrolyte, indicating that CDPZ@G electrode possesses obvious Na^+ storage behaviors and superior electrochemical performance in NaOH aqueous electrolyte. Therefore, 10 M NaOH aqueous electrolyte has been employed as the suitable electrolyte of CDPZ@G electrode in our work.

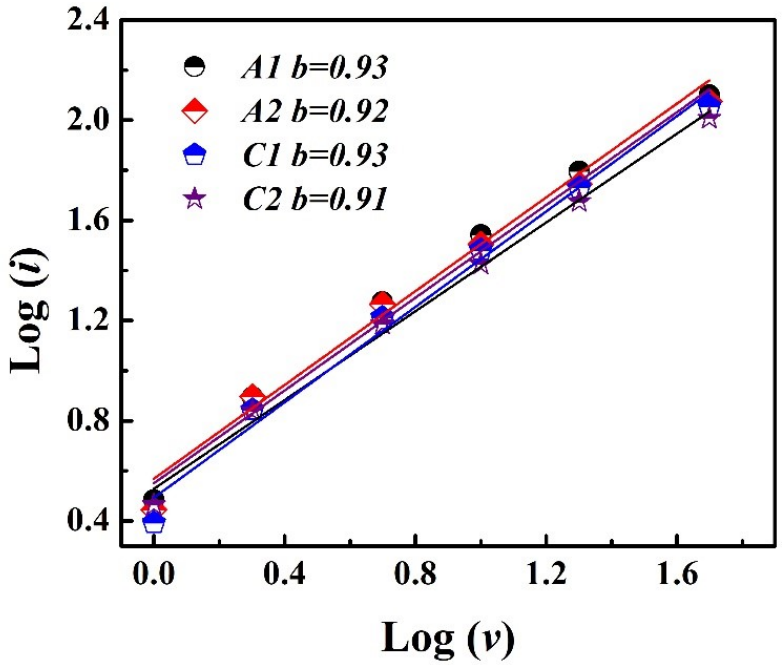

Fig. S4 Plots of log(*i*) *vs.* log(*v*) obtained from the redox peak currents in CV curves of the CDPZ@G electrode.\

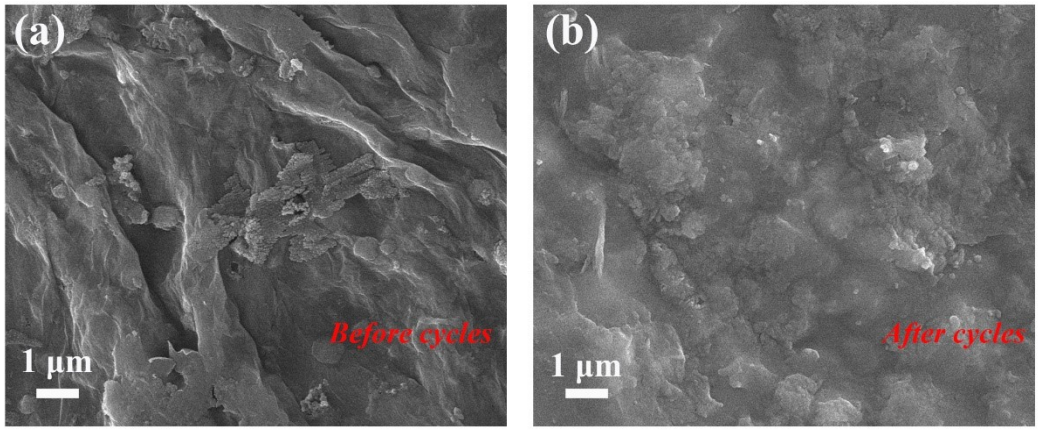

Fig. S5 SEM images of CDPZ@G electrode before and after cycles.

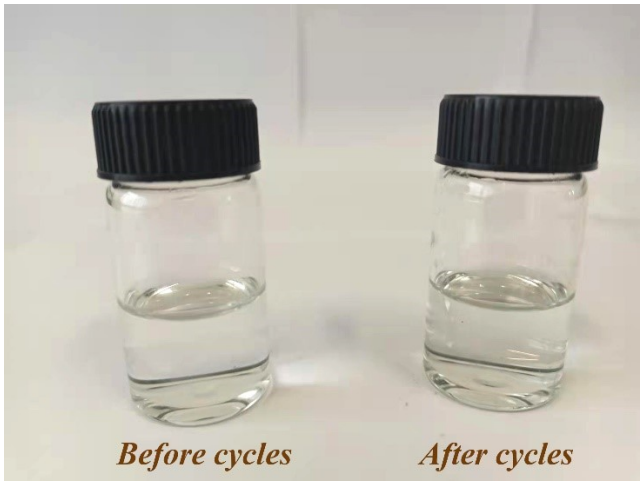

Fig. S6 Digital photos of the corresponding dissolution of CDPZ@G electrode before and after cycles.

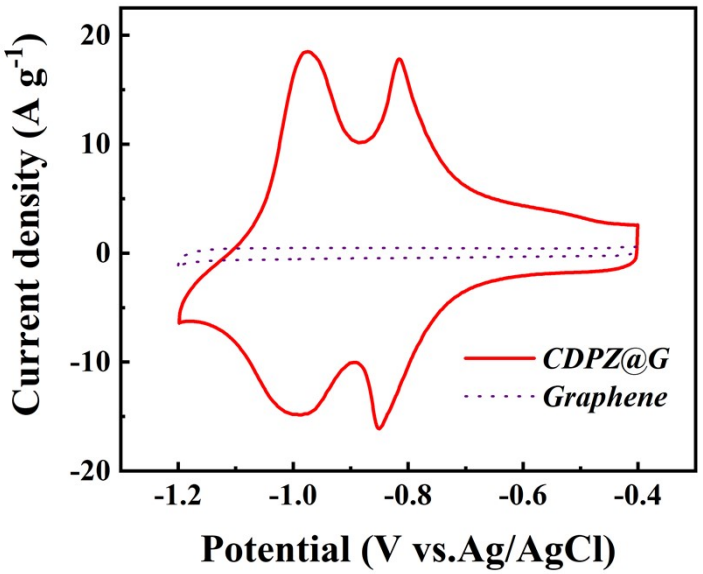

Fig. S7 CV curves for the graphene and CDPZ@G electrodes in NaOH aqueous electrolyte (Ag/AgCl as reference electrode).

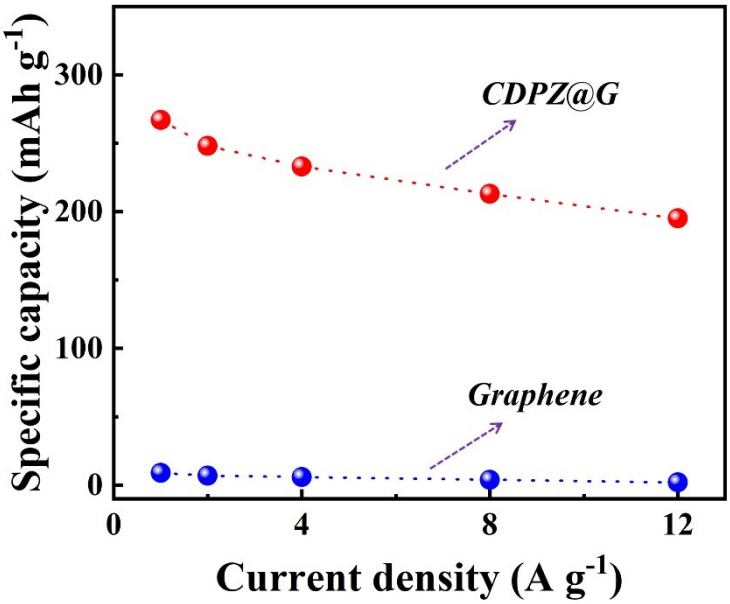

Fig. S8 Specific capacities of graphene and CDPZ@G electrodes in NaOH aqueous electrolyte under various current densities (Ag/AgCl as reference electrode).

Fig. S7 shows the CV curves of the graphene and CDPZ@G electrodes in NaOH aqueous electrolyte at a scanning rate of 5 mV s^{-1}. Compared with the rectangular-like CV curve (dotted line) of the graphene electrode, two pairs of obvious redox peaks are

observed in the curve of CDPZ@G electrode, indicating the redox behavior of CDPZ@G electrode is mainly caused by the reversible redox reaction of electro-active CDPZ unit rather than graphene. Furthermore, we have measured the specific capacities of graphene and CDPZ@G electrodes in NaOH aqueous electrolyte under various current densities. As shown in Fig. S8, the CDPZ@G electrode exhibits astonishing specific capacity with superior Na-ion storage behaviors, while graphene processes negligible capacity in NaOH aqueous electrolyte, suggesting the addition of graphene makes little contribution to the capacity of the CDPZ@G electrode. According to the above results, the capacity of the composite electrode is mainly provided by the electro-active CDPZ unit rather than graphene.

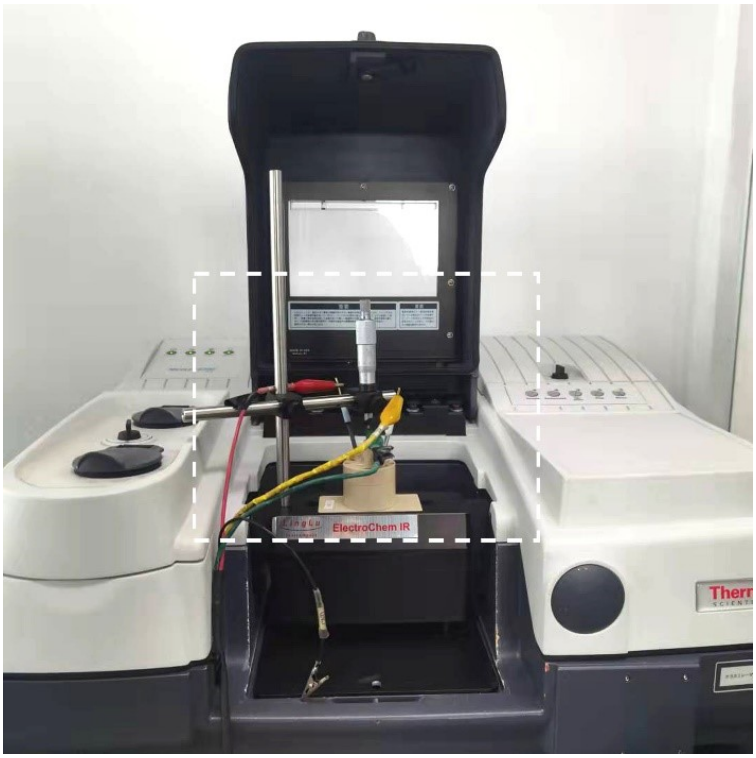

Fig. S9 Digital photo of in-situ FTIR system combined with electrochemical measurement.

In-situ ATR-FTIR measurement was carried out using a Nicolet 6700 spectrometer equipped with a mercury cadmium telluride (MCT) detector. As shown in Fig. S9, a custom-made in-situ FTIR configuration was set up with the CDPZ@G electrode pressed against a silicon crystal, wherein the infrared light is reflected on the CDPZ@G electrode surface to obtain FTIR spectra upon GCD measurement.

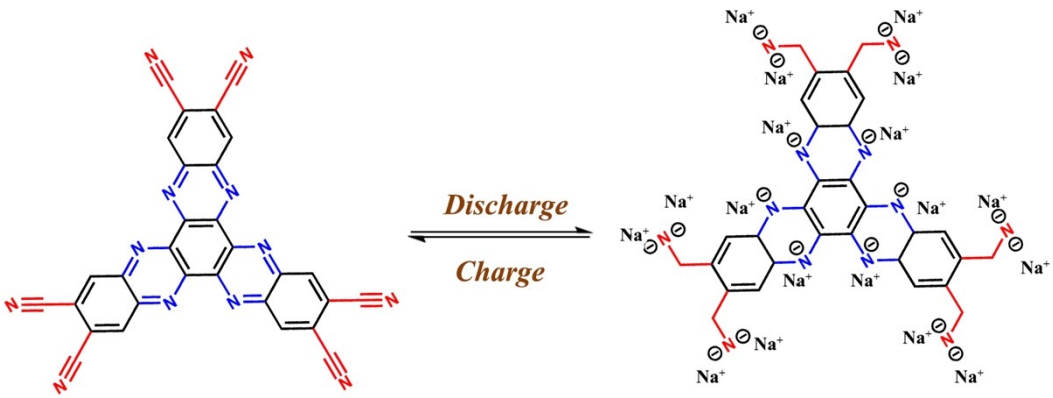

Fig. S10 Redox storage mechanism of the CDPZ upon Na^+ uptake/removal.

Fig. S10 depicts the possible redox mechanism of the CDPZ upon Na^+ uptake/removal. During the discharging process, every C=N bond from the imino moieties (bule region) and C≡N bond from the cyano substituents (red region) in CDPZ molecule can gain electrons to be reduced to C-N-Na upon Na^+ coordination. During the subsequent charging process, Na^+ removes out of the CDPZ molecule with the loss of electrons, leading to the reinstatement of CDPZ molecule occurred after fully charging. With redox-active cyano substituents and imino moieties, the CDPZ organic electrode undergoes multiple reversible redox reactions upon Na^+ uptake/removal during the charging-discharging process, which is also confirmed by the corresponding in-situ FTIR result in Fig. 3b.

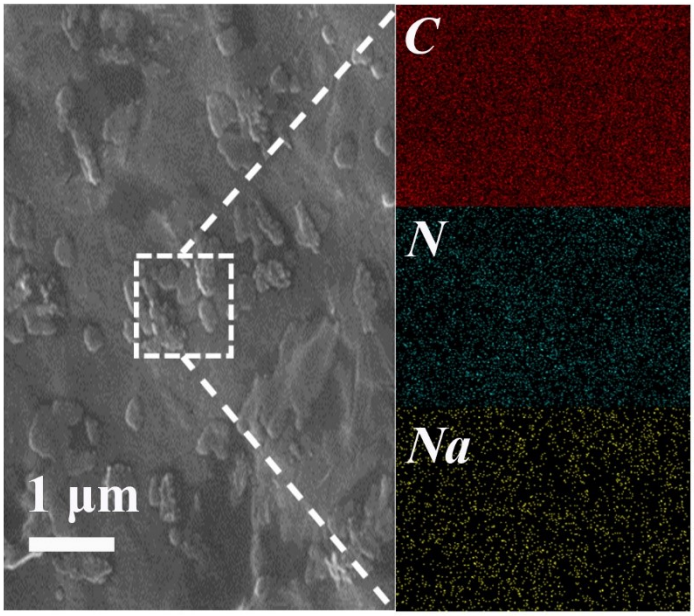

Fig. S11 SEM image and the corresponding EDS mapping images of CDPZ@G electrode at fully discharged states.

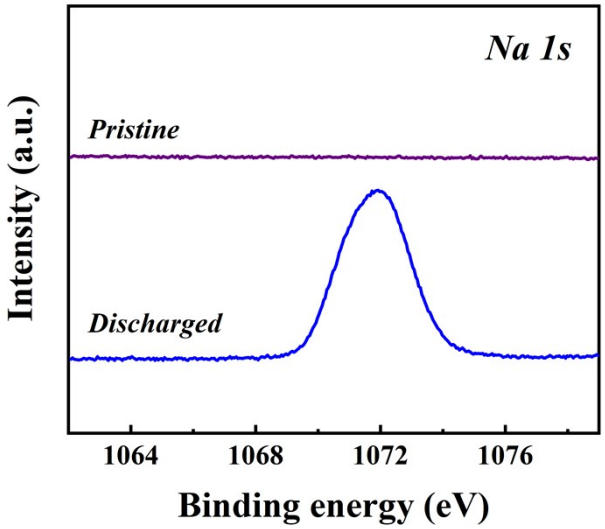

Fig. S12 XPS spectra of Na 1s at pristine and fully discharged states.

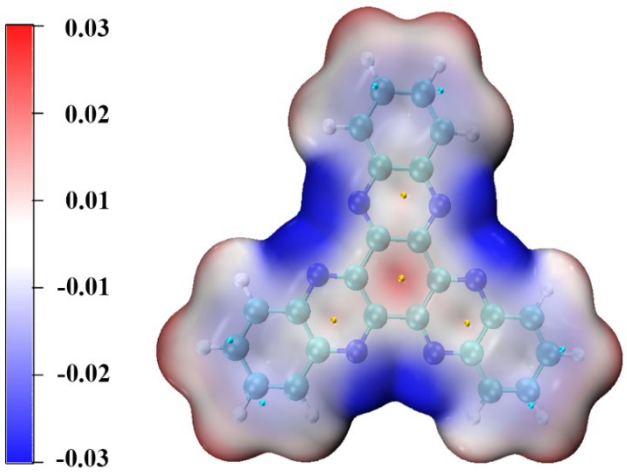

Fig. S13 MESP distribution of DPZ molecular.

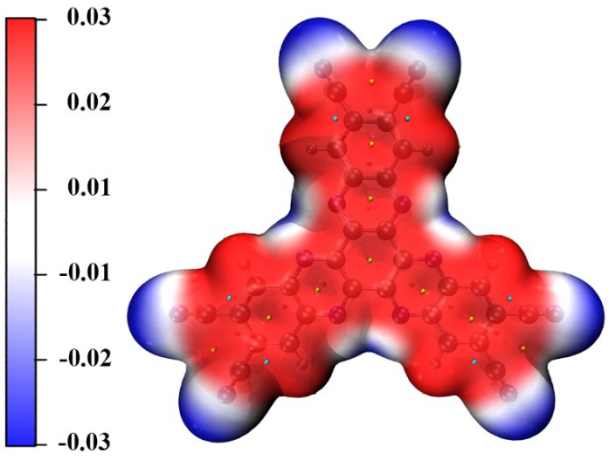

Fig. S14 MESP distribution of CDPZ molecular.

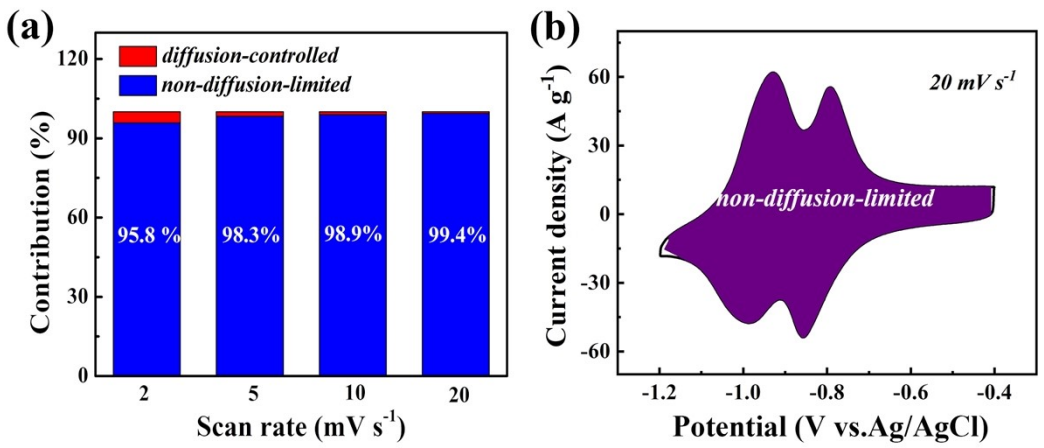

Fig. S15 (a) Capacity contributions of CDPZ@G electrode under various scan rates. (b) Voltammetric responses at the sweeping rate of 20 mV s^{-1} (Ag/AgCl as reference electrode).

To disclose the electrochemical process of the CDPZ@G electrode, the proportion of capacitive contribution can be generally quantified by the following formula:

$$i(V) = k_1 v + k_2 v^{1/2} \qquad (2)$$

where $i(V)$ is the total current at a specific potential, v the scan rate (mV s^{-1}), and $k_1 v$ and $k_2 v^{1/2}$ represent the current resulting from the capacitive-controlled and diffusion-controlled processes, respectively.

After dividing both sides of equation (2) by $v^{1/2}$, the above equation can be adjusted as follows:

$$i(V)/ v^{1/2} = k_1 v^{1/2} + k_2 \qquad (3)$$

By plotting $i(V)/ v^{1/2}$ *vs.* $v^{1/2}$, one easily derives the values of k_1 and k_2 in equation (2) as the slope and intercept of longitudinal axis and obtains the values of $k_1 v$ and $k_2 v^{1/2}$ from equation (3), which can isolate the respective contribution ratios of capacitive-controlled and diffusion-controlled processes in the CDPZ@G electrode under different scan rates. In Fig. S15a, the values of non-diffusion-limited contribution are all higher than 95.0% at various scan speeds, varying from 95.8% at 2 mV s^{-1} to 99.4% at 20 mV s^{-1} (Fig. S15b), showing the rapid storage process in CDPZ@G electrode.

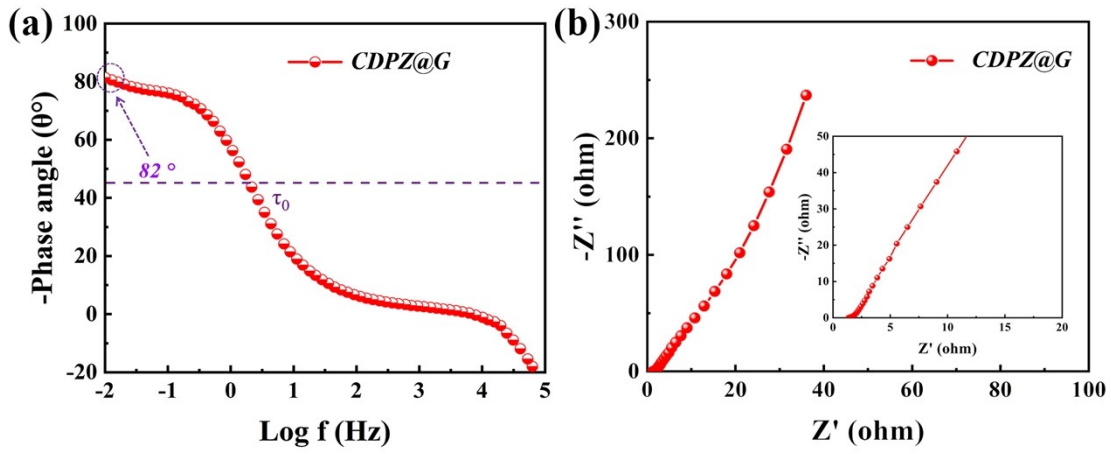

Fig. S16 (a) Bode plot and (b) EIS plot of the CDPZ@G electrode.

For a more detailed analysis about electrochemical kinetics of CDPZ@G electrode, the frequency dependent phase angle of Bode plot is depicted in Fig. S16a, in which the phase angle is about 82° that is close to the ideal phase angle (90°), indicating the fast ionic diffusion in the CDPZ@G electrode. Moreover, the relaxation time constant (τ_0) is calculated as low as ~0.49 s, suggesting the superior charge-transfer characteristic of CDPZ@G electrode. The impressive kinetics is also indicated by the electrochemical impedance spectroscopy (EIS) with the high-frequency region consist of a small semicircle and the low-frequency region consist of a straight line with a large slope (Fig. S16b).

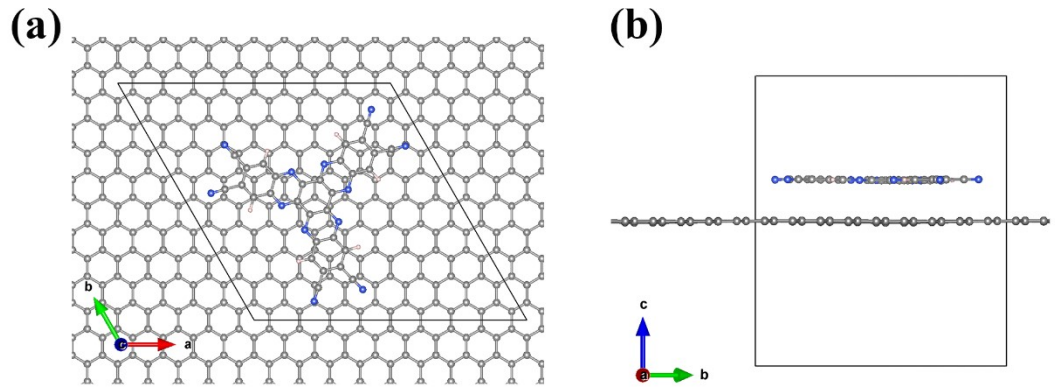

Fig. S17 DFT structures of (a) vertical and (b) front views of the CDPZ@G.

The DFT calculations were carried out using the Vienna Ab-initio Simulation Package (VASP) with the frozen-core all-electron projector-augment-wave (PAW) method. The Perdew-Burke-Ernzerhof (PBE) of generalized gradient approximation (GGA) was adopted to describe the exchange and correlation potential. The cutoff energy for the plane-wave basis set was set to 450 eV. A monolayer 9×9 graphene supercell was used. The CDPZ molecular were flat placed on 9×9 graphene supercel, and a vacuum region of 20 Å was added above the slab minimize the interactions between neighboring systems. The geometry optimizations were performed until the forces on each ion was reduced below 0.01 eV/Å. The Monkhorst-Pack k-point sampling was set to 1×1×1. The resulting structures were then used to calculate the electronic structures.

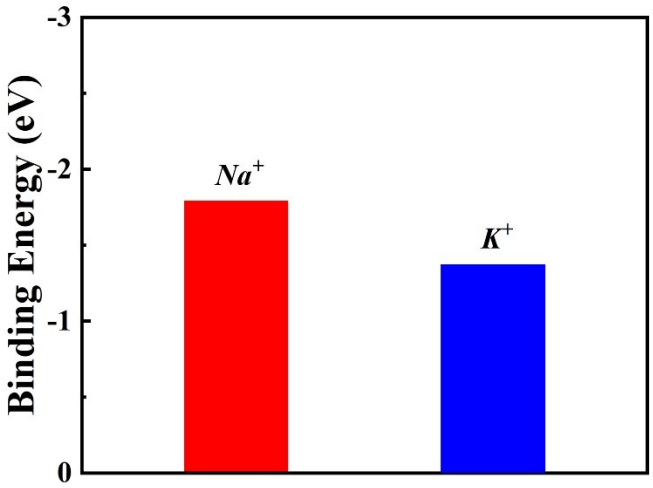

Fig. S18 Calculated Na^+ and K^+ binding energies of CDPZ molecule.

As we know, the ionic radius of Na^+ is smaller than that of K^+, indicating that uptake/removal of Na^+ from the CDPZ can occur more easily. DFT calculations have been further carried out to explore the binding energies of the CDPZ molecule coordinated with Na^+ and K^+ in aqueous electrolyte (Fig. S18). It is demonstrated that the CDPZ molecule possesses a lower Na+ binding energy of −1.79 eV compared with the K+ binding energy of −1.37 eV, indicating that the CDPZ molecule easily coordinates with Na^+ and possesses a stronger electron absorption capability.

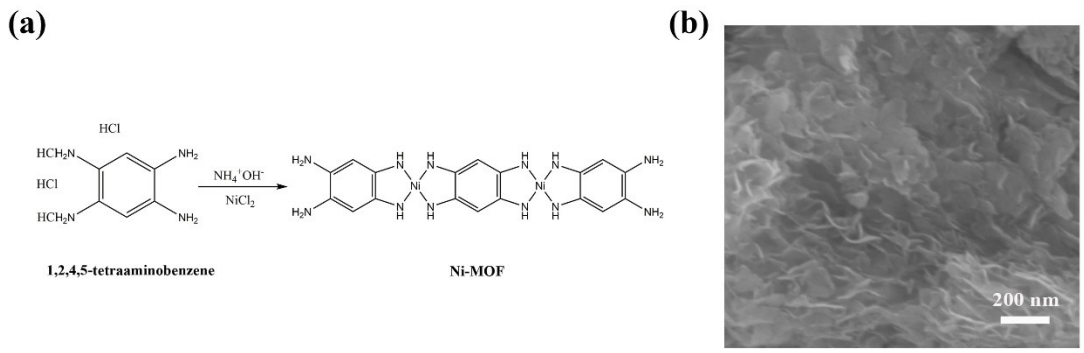

Fig. S19 (a) Schematic diagram of Ni-MOF. (b) A typical SEM image of Ni-MOF.

Fig. S19a illustrates the preparation procedure of Ni-MOF. A solution of 1 mmol $NiCl_2 \cdot 6H_2O$ in 20 mL of deionized water and 3 mL of concentrated aqueous ammonia (~14 M) were successively added to a solution of 1 mmol 1,2,4,5-tetraaminobenzene in 120 mL of water during air bubbling. After heating to 60 ℃ and stirring for 1 h, air bubbles were removed, and the mixture was still stirred for 2 h at 60 ℃. The resulting powder was isolated by filtration, washed several times with deionized water, acetone and ethanol, respectively. Fig. S19b shows the typical SEM image of the Ni-MOF with 2D nanosheets.

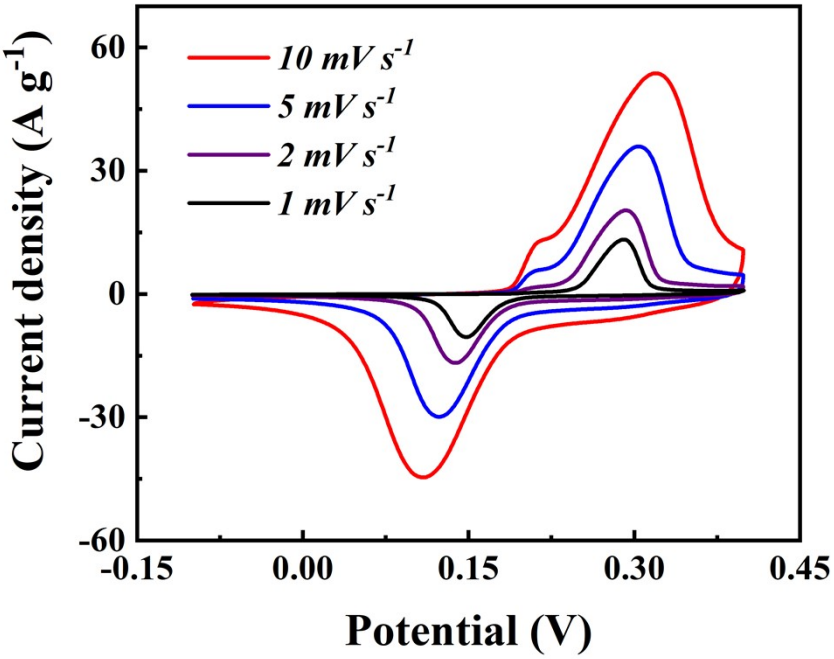

Fig. S20 CV curves at different scan rates (1~10 mV s^{-1}) of 2D Ni-MOF electrode in NaOH aqueous electrolyte (Ag/AgCl as reference electrode).